European Journal of Pharmaceutics and Biopharmaceutics 135 (2019) 1–12

Contents lists available at ScienceDirect

European Journal of Pharmaceutics and Biopharmaceutics

journal homepage: www.elsevier.com/locate/ejpb

Research paper

# Chemically identical but physically different: A comparison of spray drying, hot melt extrusion and cryo-milling for the formulation of high drug loaded amorphous solid dispersions of naproxen

Sien Dedroog[a], Christophe Huygens[b], Guy Van den Mooter[a,*]

[a] KU Leuven – University of Leuven, Department of Pharmaceutical and Pharmacological Sciences, Drug Delivery and Disposition, Leuven B-3000, Belgium
[b] Laboratoires SMB S.A., 26-28 Rue de la Pastorale, 1080 Brussels, Belgium

ARTICLE INFO

*Keywords:*
Amorphous solid dispersions (ASDs)
Spray drying
Hot melt extrusion
Cryo-milling
High drug loading

ABSTRACT

In spite of the large research efforts in the past two decades, it is still difficult, if possible at all, to predict what manufacturing technology will lead to the best amorphous solid dispersions (ASDs) in terms of drug to polymer ratio ("drug loading") and physical stability. In general, ASDs can be prepared by solvent based methods, heat based methods and mechanochemical activation. In the current study, one manufacturing technique per category was selected: spray drying, hot melt extrusion and cryo-milling, respectively. These processes were compared for their capability to formulate high drug loaded ASDs. High drug loadings may allow decreasing the pill burden and/or reducing dosage size, which both increase the therapeutic compliance. A fast crystallizer, naproxen, in combination with PVP K25, PVP-VA64, HPMC and HPMC-AS was used as a model system. Clear differences in the physical structure of the ASDs were observed. Our data indicate that not only the drug loading is dependent on the manufacturing process, but also the carrier that is able to incorporate the highest drug loading. This suggests that a carrier should be selected not only as function of the API, but also as function of the manufacturing process. Overall, hot melt extrusion showed to be most suited to reach high drug loadings for these naproxen-polymer combinations. This was in agreement with our finding that heat is an important energy input for mixing.

## 1. Introduction

A drawback of the current drug selection procedures is their high output of drug candidates with unfavorable physicochemical properties [1]. More specifically, ca. 70% of new drug candidates are poorly water soluble [2,3]. Formulation of amorphous solid dispersions (ASDs) of compounds belonging to class II and IV of the biopharmaceutics classification system (BCS) is considered as a potential strategy to tackle their solubility and dissolution rate limited bioavailability issues [1,4]. Amorphization of drug compounds results in a higher free energy compared to their crystalline form. The advantage of this higher energetic state is a higher dissolution rate and solubility, but at the same time, it is also responsible for physical stability issues like crystallization of the amorphous form. These physical stability issues can be overcome by molecularly dispersing the active pharmaceutical ingredient (API) in a polymer matrix, and thus stabilizing the API by the presence of drug–polymer interactions and by lowering the molecular mobility [5].

In general, ASDs can be prepared by solvent based methods, heat based methods, mechanochemical activation or a combination of these. Most manufacturing techniques are solvent based, such as spray drying (SD), freeze drying, electrospraying, super critical fluids based processing and bead coating. Heat based methods include melt/quench cooling and hot melt extrusion (HME), which uses both heat and shear forces as energy input [6,7]. All kinds of high energy milling are considered as mechanochemical activation. An example of such a milling technique is cryo-milling (CM) [8]. In pharmaceutical industry, both SD and HME are most commonly used. The main reason is that they are relatively easy to scale up. An additional advantage of SD is that compounds with thermal and shear instability can be formulated. On the other hand, hot melt extrusion is a solvent-free continuous process and the extrudates do not necessarily require a lot of downstream processing when a calendering step is applied [6,7,9].

Independently of the manufacturing technique used, mainly relatively low drug loadings are utilized for the development of ASDs due to

* Corresponding author at: Department of Pharmaceutical and Pharmacological Sciences, Drug Delivery and Disposition, KU Leuven – University of Leuven O&N2, Herestraat 49 Bus 921, 3000 Leuven, Belgium.
*E-mail address:* guy.vandenmooter@kuleuven.be (G. Van den Mooter).

https://doi.org/10.1016/j.ejpb.2018.12.002
Received 19 September 2018; Received in revised form 30 November 2018; Accepted 4 December 2018
Available online 05 December 2018
0939-6411/ 

potential physical stability issues. When the drug weight fraction increases, phase separation resulting in amorphous or crystalline drug precipitations may occur [7]. The importance of attaining a higher drug loading is reflected in the present-day push for a lower pill burden. By increasing the drug loading it may become possible to lower the pill burden and/or reduce the dosage size, thereby increasing the therapeutic compliance [10].

The highest drug loading possible can be predicted by calculating the maximum amount of active pharmaceutical ingredient that can be dissolved in the polymer at a certain temperature. Perturbed-Chain Statistical Associating Fluid Theory (PC-SAFT) is a thermodynamic model using the thermodynamic solid-liquid equilibrium to calculate the solubility of the API in the polymer. The liquid phase is made up of the polymer together with the dissolved API, while the solid phase is the crystalline API. Combining the calculated solubilities and the experimentally determined glass transition temperatures (Tgs), state diagrams for the solubility of the API in a specific polymer can be established [11,12].

An ASD is thermodynamically stable as long as the drug loading does not exceed the solubility of the API in the polymer, meaning that the API will never crystallize. On the other hand, higher drug loadings than the solubility limit can be reached due to kinetic stabilization. By kinetically trapping the API in the polymer matrix, the molecular mobility of the API is reduced [5,12]. The phenomena by which kinetic trapping is achieved differ between manufacturing techniques. Both rapid solvent evaporation and rapid cooling can kinetically trap the API, using solvent based and heat based methods, respectively [7,13]. Therefore, it should be possible to reach higher drug loadings experimentally than the ones predicted with a thermodynamic model.

Although the research in ASDs already started in the mid-sixties of the previous century [6,14], today it is not clear what manufacturing technology is the most suited for a given API-polymer combination. This is an important observation in the light of high drug loaded ASDs. In this paper, the differences between manufacturing techniques for their capability to obtain high drug loadings are described. Three technologies were selected: spray drying, hot melt extrusion and cryo-milling. With this selection, all categories of manufacturing techniques are covered. The novelty of this paper clearly lies in the comparison of the most relevant technologies from all three categories of manufacturing techniques.

Next to the manufacturing technique, the API-polymer combination is a critical factor for reaching high drug loadings [6]. Naproxen, which is a fast crystallizer [15], in combination with PVP K25, PVP-VA64, HPMC and HPMC-AS was used as a model system. These polymers belong to the most commonly used carriers for the formulation of ASDs. Their structural formulas are shown in Fig. 1. As becomes clear from the state diagrams generated with PC-SAFT, the mutual solid miscibility needs to be taken into account. Thus, the state diagrams of naproxen and PVP K25, PVP-VA64 or HPMC-AS served as a starting point for determining the highest drug loading experimentally (Fig. 2) [11,12]. The diagram of naproxen and HPMC was not yet described in literature.

Since interactions can also have an influence on the physical stability, the model system was selected based on its interaction potential. Formation of hydrogen bonds between the molecularly dispersed API and the polymer is of great importance for the stabilization of ASDs [5]. Naproxen is well known for its capability to form hydrogen bonds [16,17]. Its carbonyl group and methoxy group are hydrogen acceptors for the hydroxyl groups of HPMC and HPMC-AS. On the other hand, its hydroxyl group can hydrogen bond with both the carbonyl groups of PVP, PVP-VA and HPMC-AS and the hydroxyl groups of HPMC and HPMC-AS. The hypothesis is that the physical structure resulting from different manufacturing processes, and thus the contribution of hydrogen bonds to solid state miscibility will vary. Therefore, the variations in phase behavior were investigated by preparing the same model system with all three techniques.

To the best of our knowledge, a study where the most relevant technologies from solvent based, heat based and mechanochemical activation techniques are compared, has never been carried out before. The objective of this study was to prepare the same API-polymer combinations with spray drying, hot melt extrusion and cryo-milling. Hereby, the differences in capability of reaching high drug loadings were investigated. Since the API-polymer combination is a crucial factor in attaining high drug loadings, it was evaluated for four different polymers.

## 2. Materials & methods

### 2.1. Materials

Naproxen (NAP) was purchased from SA Fagron NV (Waregem, Belgium) and both polyvinylpyrollidon K25 (PVP K25, Kollidon®) and polyvinylpyrollidon vinyl acetate 64 (PVP-VA64) were obtained from BASF® ChemTrade GmbH (Ludwigshafen, Germany). Hydroxypropylmethycellulose acetate succinate (HPMC-AS) grade LF is a micronized grade of HPMC-AS, which was purchased from Shin-Etsu (Plaquemine, USA). The fourth polymer, hydroxypropylmethylcellulose (HPMC), was obtained from Colorcon (Dartford, UK). Methanol (MeOH) and dichloromethane (DCM) 99.9% were purchased from ACROS Belgium (Geel, Belgium). All materials were used as received.

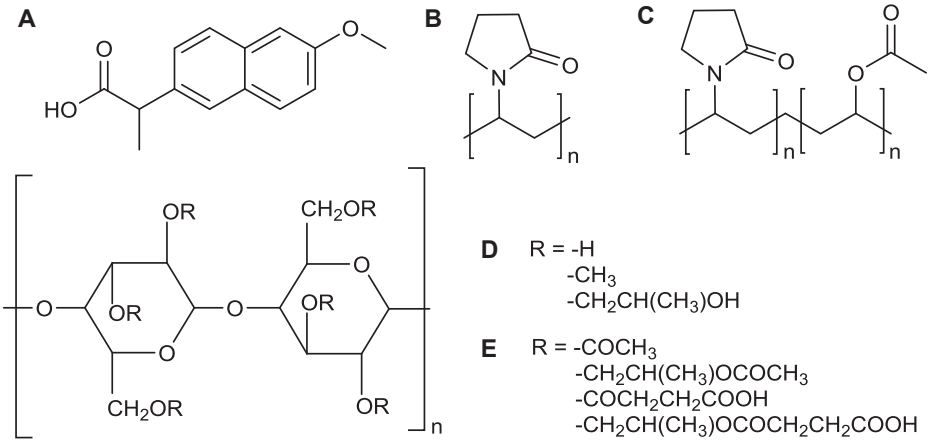


**Fig. 1.** Structural formulas of naproxen (A), PVP (B), PVP-VA (C), HPMC (D) and HPMC-AS (D, E).

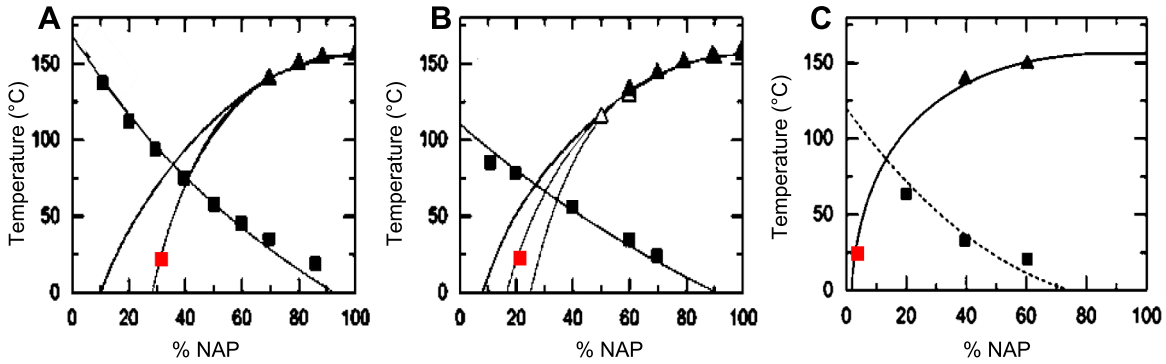


**Fig. 2.** State diagrams of NAP with PVP K25 (A), PVP-VA64 (B) and HPMC-AS (C). The black squares indicate the Tgs and the triangles the solubility of NAP in the polymer. The solubilities were determined experimentally (A, C) or taken from literature (B). Here, the white triangles were derived from Kyerematen et al. [29] and the black ones from Prudic et al. [30]. For PVP and PVP-VA, Flory-Huggings and an empirical model were applied as well. The lines with the red squares represent the solubilities calculated with PC-SAFT. These indicate the solubility of NAP in the polymer at RT. Reprinted (adapted) with permission from Lehmkemper et al. [11] *'Impact of Polymer Type and Relative Humidity on the Long-Term Physical Stability of Amorphous Solid Dispersions', Molecular Pharmaceutics, 14(12), pp. 4374–4386.* Lehmkemper et al. [12] *'Long-Term Physical Stability of PVP- and PVPVA-Amorphous Solid Dispersions', Molecular Pharmaceutics, 14(1), pp. 157–171).* Copyright 2017 American Chemical Society. (For interpretation of the references to colour in this figure legend, the reader is referred to the web version of this article.)

### 2.2. Preparation methods

#### 2.2.1. Spray drying

Diverse ratios of NAP and polymer were spray dried using a Buchi mini spray dryer B-190 (Buchi, Flawil, Switzerland). In all cases, a 10% m/v solid content was used. For the batches with PVP, PVP-VA and HPMC-AS, MeOH was used as a single solvent. For the ones with HPMC, a binary solvent mixture of MeOH:DCM (1:1; v:v ratio) was needed. The following conditions were applied: drying air temperature of 65 °C, drying air flow rate of 33 $m^3$/h, feed solution flow rate of 5 mL/min and an atomization air flow rate of 10 L/min. Immediately after spray drying, the ASDs were further dried in a vacuum oven for 4 days at 40 °C. Afterwards, the samples were analyzed and further stored at -28 °C in the presence of phosphorus pentoxide.

#### 2.2.2. Hot melt extrusion

*2.2.2.1. Batch extruder.* Physical mixtures of the NAP-polymer combinations were prepared using a mortar and pestle and extruded using a Mini extruder (DSM Xplore, Sittard, The Netherlands). This is a fully intermeshing recirculating 5 $cm^3$ extruder consisting out of two co-rotating screws. The barrel temperature was set at 160 °C, which is above the melting point (Tm) of NAP (155 °C). For every batch, about 6 g was fed into the extruder and mixed for 5 min with a screw speed of 100 rpm. The extrudates were cooled on aluminum foil and milled using a laboratory cutter mill (Kika, Staufen, Germany). The milled ASDs were analyzed and further stored at −28 °C in the presence of phosphorus pentoxide.

The effect of the barrel temperature on the phase behavior of the ASDs was explored by applying a temperature of 20 °C above the glass transition temperature (Tg) of the polymer involved. The Tgs of the four polymers were determined using modulated differential scanning calorimetry (MDSC) (3.1). To take into account possible water evaporation during extrusion, the glass transition temperatures (Tgs) obtained in the second heating cycle were used as a starting point for determining the new processing temperature.

*2.2.2.2. Continuous extruder.* To evaluate the influence of additional kneading zones on the phase behavior, a ThermoFisher process 11 twin screw extruder (ThermoFisher Scientific, Karlsruhe, Germany) was used. This is a co-rotating, fully intermeshing twin screw extruder with a functional length of 40 L/D. Two kneading zones were applied. The screw speed was set at 25 rpm and the barrel temperature was kept constant at 160 °C. Herewith, 55% of NAP was extruded in combination with PVP-VA. The same combination was extruded with the Mini extruder, using the same screw speed and temperature. These extrudates were also milled using a laboratory cutter mill (Kika, Staufen, Germany), analyzed and further stored at -28 °C in the presence of phosphorus pentoxide.

#### 2.2.3. Cryo-milling

Cryogenic grinding was performed using a CryoMill (Retsch, Düsseldorf, Germany). Physical mixtures of NAP-polymer combinations were prepared using a mortar and pestle before milling. Stainless steel grinding jars of both 5 and 25 mL with two 7 mm beads and one 15 mm bead of the same material were used, respectively. To maintain a constant ball to powder ratio the amount of sample was adapted: 200 mg in case of the 7 mm beads and 1 g in case of the 15 mm one. The samples were pre-cooled for 1 min at 5 Hz, cryo-milled for 30 min at 25 Hz and intermediately cooled for 5 min at 5 Hz to avoid heating of the system. In total, six such cycles were applied. The ASDs were analyzed and further stored at −28 °C in the presence of phosphorus pentoxide.

### 2.3. Analytical methods

#### 2.3.1. Modulated differential scanning calorimetry (MDSC)

Modulated differential scanning calorimetry was performed using a Q2000 MDSC (TA Instruments, Leatherhead, UK), equipped with a refrigerated cooling system (RCS90) and applying a dry nitrogen purge with a flow rate of 50 mL/min. Calibration for temperature, enthalpy and heat capacity was carried out using indium and sapphire standards. Optimization of the modulation parameters was performed based on the quality of the Lissajous figures and the shape of the modulated heat flow. The final parameters were as follows: a linear heating rate of 2 °C/min combined with a modulation amplitude of 0.5 °C and a period of 30 s. Approximately 1–5 mg of the sample was accurately weighed into aluminum DSC pans (TA Instruments, Zellik, Belgium). For all samples, a heat-cool-heat procedure was performed to explore the influence of additional heating on the mixing efficiency. All heating cycles were executed with the above described parameters from −15 °C to 180 °C, while the cooling rate was set at 20 °C/min. DSC thermograms were analyzed using the Universal Analysis software (Version 5.5, TA Instruments, Leatherhead, UK).

#### 2.3.2. Thermogravimetric analysis (TGA)

For determining the polymer degradation temperature, a thermogravimetric analyzer SDT Q600 (TA-Instruments, Leatherhead, UK) was used. The samples were heated at 5 °C/min to 230 °C in ambient

atmosphere, where the recorded weight loss as a function of time was due to degradation. All TGA curves were analyzed using the Universal Analysis software (Version 5.5, TA Instruments, Leatherhead, UK).

### 2.3.3. X-ray powder diffraction (XRPD)

The solid state of the ASDs was characterized using a X'Pert PRO diffractometer (PANalytical, Almelo, the Netherlands) with a Cu tube (Kα λ = 1.5418 Å) and a generator set at 45 kV and 40 mA. In most cases, the XRPD measurements were executed at room temperature (RT) and in transmission mode using Kapton® Polyimide Thin-films (PANalytical, Almelo, Netherlands). In case of temperature resolved X-ray diffraction, an Anton Paar sample stage (TTK450 Sample Stage) was applied. In that case, diffractograms were recorded every 10 °C between room temperature and 180 °C. The following experimental parameters were applied in all cases: continuous scan mode from 4° to 40° 2θ with 0.0167° step size and 400 s counting time. The diffractograms were analyzed using X'Pert Data Viewer (Version 1.7, PANalytical, Almelo, The Netherlands).

## 3. Results & discussion

### 3.1. Spray drying

#### 3.1.1. Influence of NAP-polymer combination on physical structure

In a first step, the same drug loading of NAP was spray dried in combination with all four polymers. Using a drug loading of 35%, the phase behavior varied for the different NAP-polymer combinations. A single Tg was detected for the ASD with PVP-VA, while the one with PVP resulted in two Tgs (Fig. 3A). In case of a one phase amorphous system, the Tg is situated in between the Tg of the pure amorphous drug and the one from the polymer. For example for the ASD of NAP and PVP-VA, the Tg was situated at 57.1 °C, which is in between the 5 °C for amorphous NAP and 110 °C for PVP-VA (Table 1) [18].

Since the distinction between two Tgs is not always clear in the reversing heat flow (RHF) signal, we also used the derivative of this signal (Fig. 3B). In that case, a peak is generated with a maximum value corresponding to the inflection point in the RHF signal. The presence of two Tgs, reflected in two distinct peaks in the derivative RHF, indicates amorphous-amorphous phase separation in a drug-rich and a polymer-rich phase. Although the NAP-PVP system is amorphous in case of a drug loading of 35%, its immiscibility can be a precursor of crystallization, which will most likely start from the drug-rich amorphous phase. Next to its advantage for distinguishing Tgs, the derivative of the RHF signal was used for determining the Tg width. The broader this Tg width, the more heterogeneous the ASD is. Therefore, it can be stated that the broader this range, the sooner phase separation and thereby crystallization may occur.

For both the combinations with HPMC and HPMC-AS, a Tg and a Tm were observed. Here, the RHF signal is shown, but the Tms were detected in the total heat flow and non-reversing heat flow signal (data not shown). These Tms indicated the presence of a crystalline phase of NAP next to the amorphous one (Fig. 3A).

These results were in agreement with the ones obtained using XRPD. Both PVP-VA and PVP were X-ray amorphous, while both HPMC and HPMC-AS showed Bragg peaks characteristic for crystalline NAP (Fig. 4).

**Table 1**
Tgs from second heating cycle, derived processing temperatures and degradation temperatures for PVP, PVP-VA, HPMC and HPMC-AS.

| Polymer | Tg 2nd heating cycle | Tg + 20 °C | T degradation |
|---|---|---|---|
| PVP | 161.6 °C | 180 °C | 159.1 °C |
| PVP-VA | 110.8 °C | 130 °C | 197 °C |
| HPMC | 147.8 °C | 167 °C | 176 °C |
| HPMC-AS | 115.8 °C | 135 °C | 166.8 °C |

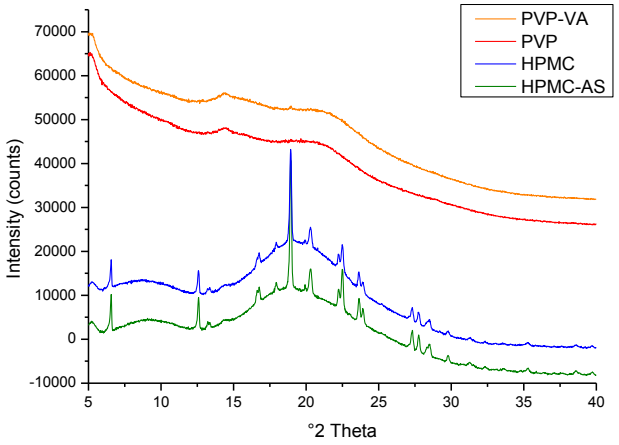


**Fig. 4.** XRPD diffractograms of 35% NAP with spray dried PVP-VA (orange), PVP (red), HPMC (blue) or HPMC-AS (green). The intensities are shown as arbitrary units. (For interpretation of the references to colour in this figure legend, the reader is referred to the web version of this article.)

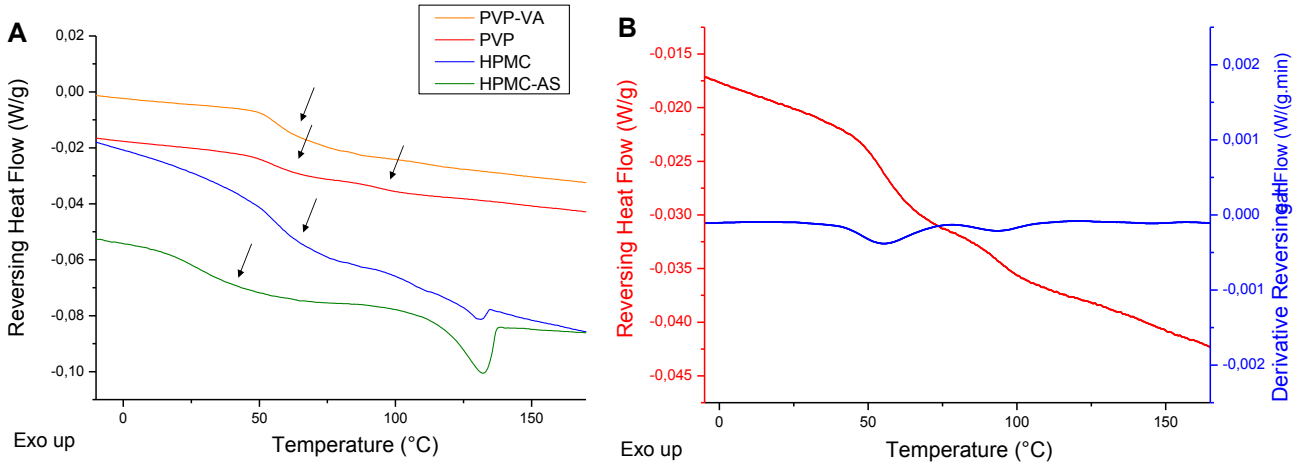


**Fig. 3.** A: MDSC thermograms of 35% NAP spray dried with PVP-VA (orange), PVP (red), HPMC (blue) or HPMC-AS (green). The arrows indicate the positions of the Tgs. The RHF signals are shown as arbitrary units. B: MDSC thermogram of 35% NAP spray dried with PVP. The derivative (blue) of the reversing heat flow (red) shows peak maximums at the Tgs. (For interpretation of the references to colour in this figure legend, the reader is referred to the web version of this article.)

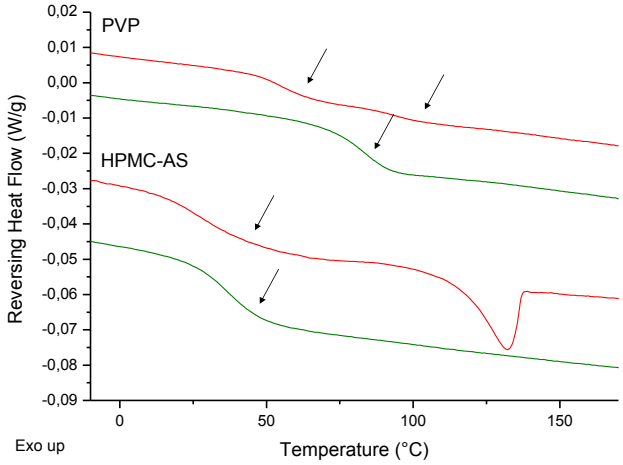


**Fig. 5.** MDSC thermograms of 35% NAP spray dried with either PVP (top) or HPMC-AS (bottom). The first heating cycle (red) and the second (green) are shown. The arrows indicate the positions of the Tgs. The RHF signals are shown as arbitrary units. (For interpretation of the references to colour in this figure legend, the reader is referred to the web version of this article.)

The importance of using complementary analytical techniques becomes clear when comparing the DSC and XRPD results. Although the same conclusions about the presence of amorphous/crystalline material can be drawn, XRPD does not give information about the different amorphous phases. Whereas the NAP-PVP system was X-ray amorphous, it was not a single amorphous phase in the MDSC thermogram. Since amorphous-amorphous phase separation can lead to crystallization, it should be avoided. Only in a one phase system the stabilization of NAP by the polymer is maximized, though not guaranteed. To get as much information about the phase behavior as possible, all samples were analyzed using both MDSC and XRPD.

For all samples, a heat-cool-heat procedure was performed to investigate the influence of additional heating on the mixing efficiency. For all of them, a single Tg was obtained in the second heating run, independently of the phase behavior in the first heating run. In case of 35% NAP spray dried with PVP, two Tgs were detected in the first heating cycle and a single Tg in the second (Fig. 5). For the combination of 35% NAP with HPMC-AS, both a Tg and a Tm could be distinguished in the first cycle and a single Tg in the second (Fig. 5). Next to this, the Tg width decreased when there already was a single Tg attained in the first heating run, indicating an increase in homogeneity of the system (data not shown). This clearly points to the importance of heat as energy input for all these NAP-polymer combinations. All further reported drug loadings were derived from the first heating cycle of the DSC experiment.

### 3.1.2. *Influence of drug loading on physical structure*

Ideally, a single amorphous phase should be obtained, in which NAP is molecularly dispersed in the polymer matrix. Since this phase behavior was only detected for the NAP-PVP-VA system, PVP-VA was appointed the most promising polymer for increasing the drug loading further. For the other combinations, the drug loading was lowered until a one phase amorphous system was achieved. The drug loading for which this ideal phase behavior was attained, was defined as 'the highest drug loading possible'. Taking into account the possible process variability, the highest drug loading was not defined as an exact percentage but as a range.

The drug loading was lowered with intermediate steps of 5% for the NAP-PVP, NAP-HPMC and NAP-HPMC-AS combinations. The MDSC and XRPD results are only described for the NAP-HPMC-AS system (Fig. 6), but the same principle has been applied for the other combinations. The highest drug loadings using the three different manufacturing techniques are summarized in Table 4.

In case of the NAP-HPMC-AS system, from 25% on, both a Tg and a Tm could be distinguished (Fig. 6A), and at 30%, Bragg peaks were present in the XRPD diffractogram (Fig. 6B). Thus, the highest drug loading for this NAP-HPMC-AS system in case of SD is in between 20% and 25%.

The NAP-PVP-VA combination was the only one for which the drug loading could be increased above 35%. It was increased from 35% until 60% with intermediate steps of 5%. Until 40% a single Tg was detected, but starting from 45% a Tm was detected next to the Tg (Fig. 7A). The MDSC results were in good correlation with the ones from XRPD, showing Bragg peaks starting from 45% drug loading (Fig. 7B). Therefore, the highest drug loading for the NAP-PVP-VA system in case of SD was in between 40% and 45%.

The four polymers can be ordered for their capability to stabilize high NAP loadings: PVP-VA > PVP > HPMC/HPMC-AS. With a drug loading between 40% and 45%, PVP-VA was the best polymer for obtaining high drug loadings. In case of PVP, the highest drug loading was between 30% and 35%, while for both HPMC and HPMC-AS it was between 20% and 25% (Table 4). It is noteworthy that these drug loadings only apply to spray drying and that variations are possible when applying other manufacturing techniques (see below).

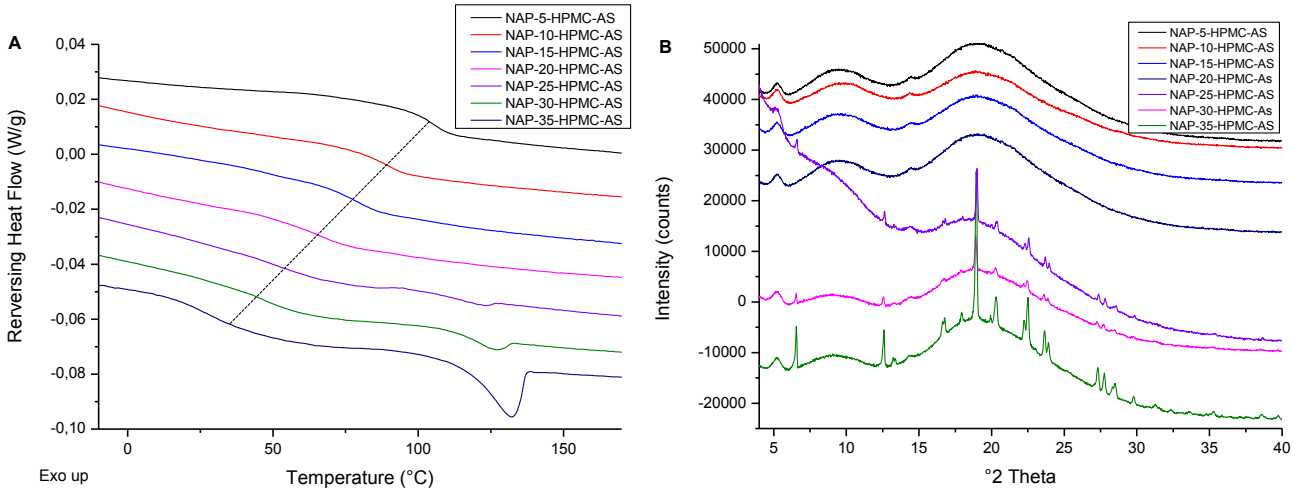


**Fig. 6.** A: MDSC thermograms of NAP-HPMC-AS system lowering the drug loading from 35% to 5% with intermediate steps of 5%. When increasing the drug loading there was a shift of the Tg towards lower values, which is indicated with the dotted line. B: Corresponding XRPD diffractograms. The RHF signals (A) and intensities (B) are shown as arbitrary units.

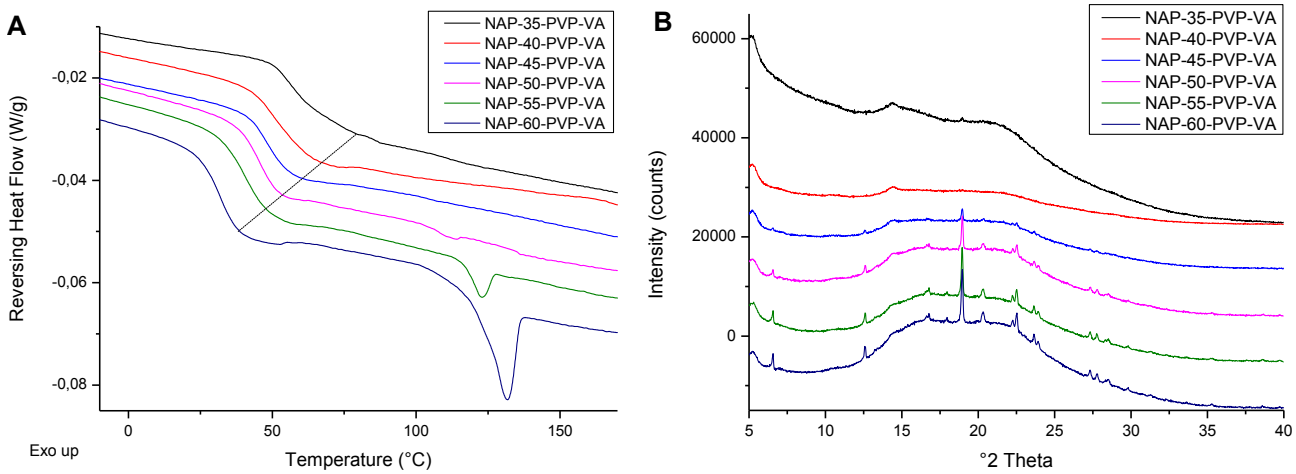


**Fig. 7.** A: MDSC thermograms of NAP-PVP-VA system increasing the drug loading from 35% to 60% with intermediate steps of 5%. When increasing the drug loading there was a shift of the Tg towards lower values, which is indicated with the dotted line. B: Corresponding XRPD diffractograms. The RHF signals (A) and intensities (B) are shown as arbitrary units.

It is expected that an API has a higher solid solubility in a polymer where drug-polymer interactions are more pronounced [19]. Therefore, this may be an indication of more favorable interactions between NAP and PVP-VA.

In this study, the main investigated characteristic is the capability to obtain high drug loadings. As described earlier, the API-polymer is a critical factor for reaching these drug loadings. Other important properties to consider when selecting a suitable polymer for SD are the common solvent solubility of API and polymer, solution state chemistry, interaction potential, antiplasticizing efficiency, dissolution rate and ability to maintain supersaturation during dissolution. Although Friesen et al. [20] described HPMC-AS as an ideal polymer for SD based on these characteristics, the drug loadings reached in this study are rather low [13]. This demonstrates that there is no ideal polymer per manufacturing technique, but that a polymer should also be selected according to the API that needs to be formulated. Other than that, it indicates that the capability to reach higher drug loadings is another important characteristic to investigate when selecting a polymer for the formulation of an ASD.

### 3.2. Hot melt extrusion

#### 3.2.1. Influence of NAP-polymer combination on physical structure

Physical mixtures of NAP with the different polymers were extruded in a 35:65 (drug:polymer; w:w) ratio. The ASDs with PVP-VA and PVP showed a single Tg, while for HPMC and HPMC-AS both a Tg and a Tm could be distinguished (Fig. 8A). Both PVP-VA and PVP are thus promising polymers for increasing the drug loading above 35%. Although the same NAP-polymer combinations and drug loading had been used as for spray drying, two NAP-polymer combinations could be formulated as a single phase amorphous system instead of one, showing that the suitability of NAP-polymer combinations depends upon the applied manufacturing technique.

All four NAP-polymer combinations were X-ray amorphous for a drug loading of 35% (Fig. 8B). Despite the fact that a Tm could be detected in the thermograms of the combinations with HPMC and HPMC-AS, there were no Bragg peaks present in the diffractograms, pointing again to the importance of using complementary analytical techniques.

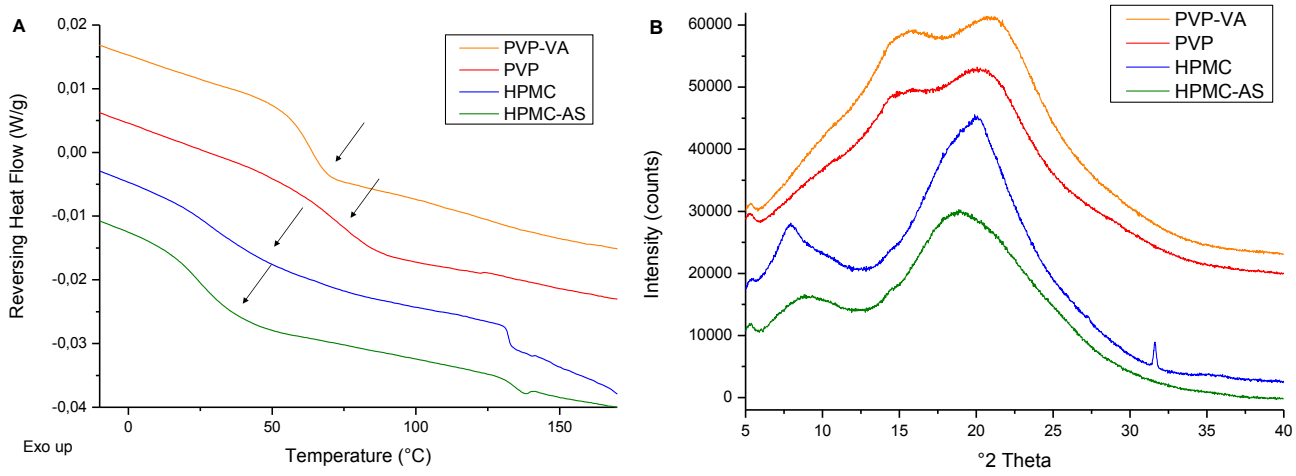


**Fig. 8.** A: MDSC thermogram of 35% NAP extruded with PVP-VA (orange), PVP (red), HPMC (blue) or HPMC-AS (green). B: XPRD diffractograms of 35% NAP extruded with PVP-VA (orange), PVP (red), HPMC (blue) or HPMC-AS (green). The sharp peak in the diffractogram of the ASD with HPMC originates from a crystalline impurity present in the polymer. The RHF signals (A) and intensities (B) are shown as arbitrary units. (For interpretation of the references to colour in this figure legend, the reader is referred to the web version of this article.)

### 3.2.2. Influence of drug loading on physical structure

In case of HME, the drug loading was increased for the NAP-PVP-VA and NAP-PVP systems, but decreased in case of the NAP-HPMC and NAP-HPMC-AS systems to obtain a one phase amorphous system. A full comparison of the highest drug loadings reached per polymer and per manufacturing technique is shown in Table 4.

### 3.2.3. Impact of polymer-dependent-barrel temperature on the physical structure

Critical process parameters for HME are the screw speed, screw configuration, feeding rate and barrel temperature. The interested reader is referred to excellent reviews for further information [21,22]. In view of using different NAP-polymer combinations, the barrel temperature is a crucial parameter. Since a polymer needs to be extruded above its Tg but below its degradation temperature, different temperatures should be applied for the different NAP-polymer combinations. The temperature is also of importance for processing of the API, but it can be processed below or above its Tm, resulting in solubilization or miscibility of the API in the polymer, respectively [22,23].

First, the degradation temperatures of the four polymers were determined using TGA (Table 1). Next to this, the Tgs of the polymers and Tm of pure NAP were taken into account. The Tgs of the polymers were determined from the second heating cycle of the MDSC run to take possible water evaporation during HME into account (Table 1). The Tm of NAP was established at 155.2 °C (data not shown).

Since the degradation temperature and Tg of PVP are comparable to each other, PVP is known to be a difficult polymer for extruding. When heated to 150 °C, darkening of PVP is described [24]. On the other hand, when increasing the temperature from 160 °C to 230 °C, only 2% degradation of PVP was measured during the TGA experiment. Thus, only a very small amount of PVP was degraded at 160 °C. For the other polymers, the degradation temperatures were well above their Tgs.

All NAP-polymer combinations were processed both at 160 °C and at 20 °C above the Tg of the polymer in question (Table 1). The barrel temperature of 160 °C was installed as a common processing temperature. For PVP-VA and HPMC-AS the Tg-dependent-temperature was below the Tm of NAP, while for PVP and HPMC it was even higher than 160 °C. By using these barrel temperatures, the influence of processing below or above the Tm of NAP on the final phase behavior was evaluated.

The results from both processing at 160 °C and at the Tg-dependent-temperature are shown in Table 2. For the cases with a barrel temperature of 160 °C, the values for the Tgs and Tms correlate with the MDSC thermograms shown in Fig. 5A. In view of the clear differences in phase behavior for the NAP-PVP-VA combination, these MDSC results are discussed more comprehensively (Fig. 9).

When processing above the Tm of NAP, no clear differences in phase behavior could be detected. Despite the fact that there was a shift of the Tg towards a lower temperature, a single Tg remained in case of PVP. With HPMC, a Tg and a Tm were detected for both 160 °C and 167 °C.

**Table 2**
Influence of HME processing temperature below/above Tm NAP on the phase behavior of the ASD. The 'X' indicates that there was no second Tg or a Tm present.

| Polymer | Temperature | Tg1 | Tg2 | Tm |
|---|---|---|---|---|
| PVP | 160 °C | 80.4 °C | X | X |
| | Tg + 20 °C | 56.2 °C | X | X |
| PVP-VA | 160 °C | 63.6 °C | X | X |
| | Tg + 20 °C | 45.4 °C | 80.4 °C | X |
| HPMC | 160 °C | 27.8 °C | X | 127.9 °C |
| | Tg + 20 °C | 26.5 °C | X | 126.5 °C |
| HPMC-AS | 160 °C | 24.3 °C | X | 128.1 °C |
| | Tg + 20 °C | 25.2 °C | X | 126.5 °C |

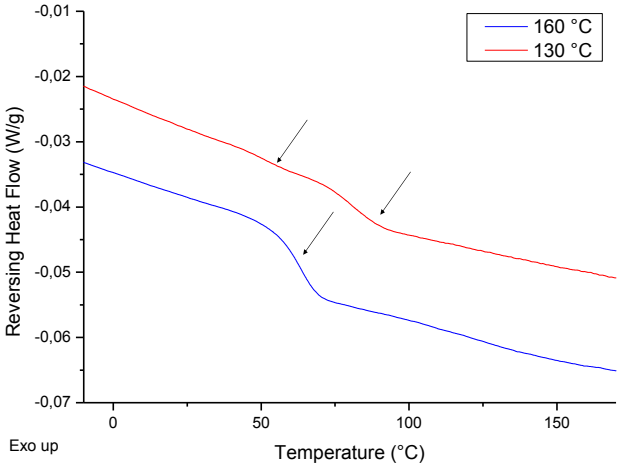


**Fig. 9.** MDSC thermograms of 35% NAP in combination with PVP-VA at 130 °C (green) and 160 °C (red). Tgs are indicated with arrows. The RHF signals are shown as arbitrary units. (For interpretation of the references to colour in this figure legend, the reader is referred to the web version of this article.)

When processing below the Tm of NAP with HPMC-AS, almost no differences in phase behavior were detected. At both processing temperatures, 160 °C and 135 °C, a Tg and a Tm could be distinguished. On the other hand, in case of PVP-VA, the phase behavior clearly differed. The amorphous-amorphous phase separation indicated that extruding at temperatures lower than the Tm of NAP did not give the system its full capability of both mixing and solubilizing the API in the polymer matrix. This is an important observation in the light of reaching high drug loadings. It is clear that for some API-polymer combinations it is important that the barrel temperature is installed above the Tm of the API. Therefore, all other batches were processed at 160 °C to give the systems their full potential to mix and thereby reach high drug loadings.

### 3.2.4. Impact of kneading zones on amorphization

In a HME process, the combination of mixing and melting makes the generation of ASDs possible. For this, two important energy inputs need to be taken into account. First, the heat conduction from the barrel will have an influence on the melting and softening process, which is determined by the installed barrel temperature. Second, the rotation of the screws will result in shear forces that will generate additional heat. This energy input can be altered by changing the screw configuration. Thus, the screw configuration is another critical process parameter. Several studies investigated the need for one or more kneading zones during HME. Nakamichi et al. [25] concluded that at least one mixing zone was needed to make amorphization possible. Saerens et al. [26] showed that addition of a second or third kneading zone did not have an additional advantage for the formulation of ASDs. Hence, one kneading zone at two third of the barrel length is in many cases considered sufficient for mixing at molecular level [22].

In contrast to a continuous extruder, a typical lab-scale batch extruder has no additional kneading zones, but exists out of two conical screws with conveying elements. Therefore, there is no alteration of the screw configuration possible. To evaluate the addition of kneading zones on the final phase behavior of the ASDs, a continuous extruder was used.

The reasoning behind the addition of kneading zones for reaching higher drug loadings becomes clear when comparing the different MDSC heating cycles. Every MDSC experiment existed out of two heating cycles separated by a cooling cycle. As described for spray drying, the second heating cycle resulted in ideal phase behavior. Despite the fact that there were two Tgs or a Tg and a Tm in the first heating cycle, a single Tg was detected in the second one. A

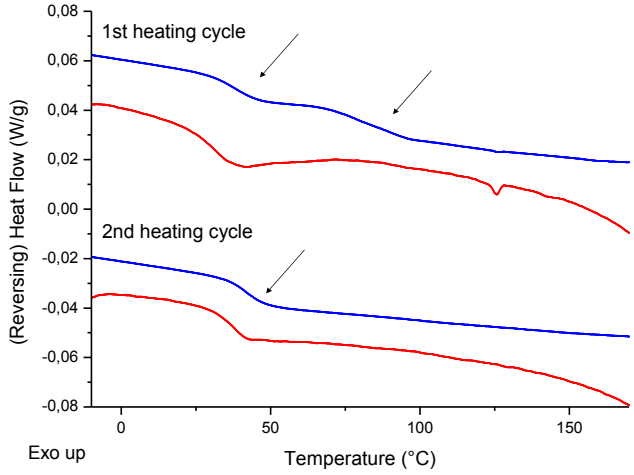


**Fig. 10.** MDSC thermograms of 55% NAP extruded in combination with PVP-VA. Both the reversing heat flow (blue) and the total heat flow (red) are shown. The arrows indicate the position of the Tgs. The (R)HF signals are shown as arbitrary units. (For interpretation of the references to colour in this figure legend, the reader is referred to the web version of this article.)

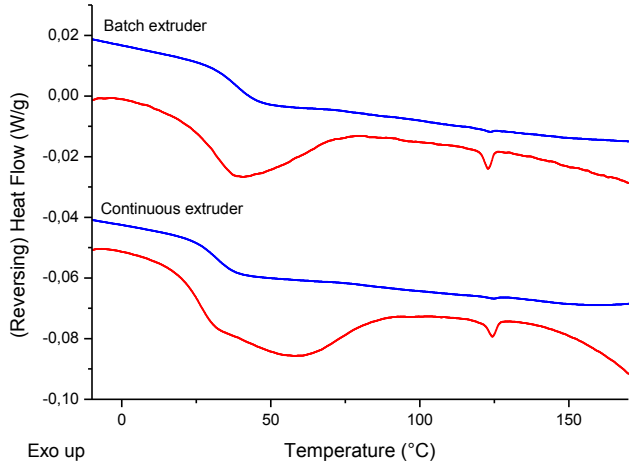


**Fig. 11.** MDSC thermograms of 55% NAP extruded in combination with PVP-VA using a batch extruder or a continuous extruder. The reversing heat flow is shown in blue and the total heat flow in red. The (R)HF signals are shown as arbitrary units. (For interpretation of the references to colour in this figure legend, the reader is referred to the web version of this article.)

representative example of HME is shown for which 55% NAP was extruded in combination with PVP-VA. Here, two Tgs and a Tm were detected in the first heating cycle and a single Tg was observed in the second (Fig. 10). This implies that heat is a very important energy input to obtain ASDs of NAP.

Since the energy input can be increased by the addition of kneading zones next to the conveying zones, we evaluated the use of a continuous extruder to prepare ASDs made up of 55% NAP and PVP-VA. The screw speed was set at 25 rpm and the process temperature at 160 °C. An additional batch was prepared with the lab scale extruder, using the same screw speed and process temperature to compare the two processes. In both cases, a Tg and a Tm were detected (Fig. 11). The amount of crystallinity was calculated from the heat of fusion, resulting in 0.6% crystallinity in both cases. Thus, it was not possible to reach higher drug loadings using the continuous extruder. This suggested that the addition of kneading zones did not result in enough energy input to increase the amorphization capability.

Lang et al. [27] compared a single screw extruder, a small twin screw extruder and a continuous twin screw extruder with kneading zones for the formulation of ASDs. They observed that only the continuous twin-screw extruder with additional kneading zones resulted in ASDs of itraconazole with HPMC-AS and PEO. In this study, similar results were obtained with the lab-scale extruder and the continuous extruder, pointing to the potential of the former. However, another explanation for the comparable results could be the remaining differences in processing time, e.g. the mixing time/residence time of 5 min in the batch extruder compared to that in the continuous process. No exact measurements of the residence time in the continuous extruder have been made, but it is clear that the total time inside the extruder is far less than 5 min. Therefore, it can be stated that a full comparison of a batch and a continuous extruder requires optimization of both processes to make the correct conclusions about their capability of reaching high drug loadings.

### 3.3. Cryo-milling

#### 3.3.1. Influence of NAP-polymer combination on physical structure

Physical mixtures of 35% NAP in combination with all four polymers were cryo-milled. The experiments were performed with small grinding jars of 5 mL, 200 mg powder mass and 2 beads of 7 mm per grinding jar. The MDSC results showed two Tgs for the combination with PVP-VA and one Tg for the one with PVP (Fig. 12A). This indicates that in case of CM, PVP is the most promising polymer for increasing the drug loading higher than 35%. For SD this was PVP-VA, while for HME it were both PVP and PVP-VA. This shows again that the success rate of an API-polymer combination clearly depends upon the manufacturing technique used. For both combinations with HPMC and HPMC-AS, a Tg and a Tm were detected (Fig. 12A).

Despite the fact that the thermograms of the combinations with PVP-VA and PVP did not show crystallinity (only glass transitions could be observed), the corresponding diffractograms showed diffraction peaks that are characteristic for crystalline NAP (Fig. 12B). This is in contradiction with the higher sensitivity of MDSC compared to XRPD for the detection of crystallinity. For the other two combinations, the MDSC and XRPD results were in good agreement with each other, indicating the presence of crystalline NAP (Fig. 12B).

The hypothesis to explain this discrepancy between MDSC and XRPD results was that by cryo-milling the particle size was reduced significantly, leading to improved particle-particle contact. Hence, only a small amount of heat was necessary to dissolve NAP in the polymer. This was further confirmed by performing temperature resolved XRPD for the NAP-PVP combination, where the temperature was increased from RT to 185 °C and a diffractogram was assessed every 10 °C. At RT, Bragg peaks indicating the presence of crystalline NAP were present. The intensity of the peaks was identical at 75 °C, but decreased at 85 °C. From 95 °C, the Bragg peaks completely disappeared, indicating that the sample was X-ray amorphous (Fig. 13). This validated the hypothesis that heating up the sample resulted in dissolving NAP particles in the polymer matrix. The need for complementary analytical techniques becomes clear when comparing these MDSC and XRPD results. When MDSC would have been used as the only analytical technique, CM might have seemed as promising as SD. A drawback of MDSC is that the sample needs to be heated, which can alter the characteristics of the analyzed sample. Thus, in this case XRPD is a more trustworthy technique to draw conclusions about the phase behavior of the cryo-milled samples at RT. Bikiaris et al. [28] reported a similar case, where Felodipine dissolved in PEG during the DSC experiment, while diffraction peaks were present in the diffractograms.

A comparison of the obtained drug loadings using MDSC or XPRD is shown in Table 3. In case of MDSC, the highest drug loading was defined as the one for which a one phase amorphous system was attained, while for XRPD the sample had to be X-ray amorphous. Although the obtained drug loadings were clearly lower using XRPD, PVP was in both cases the most suited polymer for obtaining high drug loadings. For comparison with spray drying and hot melt extrusion, the drug loadings based on XRPD results were used (Table 4).

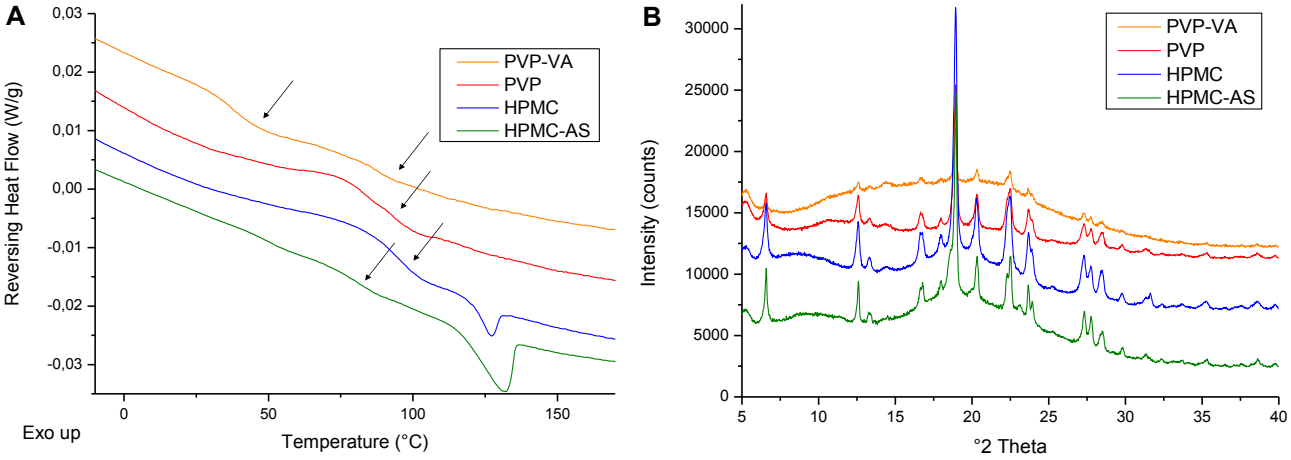


**Fig. 12.** A: MDSC thermograms of 35% NAP extruded with PVP-VA (orange), PVP (red), HPMC (blue) or HPMC-AS (green). The arrows indicate the position of the Tgs. B: XRPD diffractograms of 35% NAP cryo-milled with PVP-VA (orange), PVP (red), HPMC (blue) or HPMC-AS (green). (For interpretation of the references to colour in this figure legend, the reader is referred to the web version of this article.)

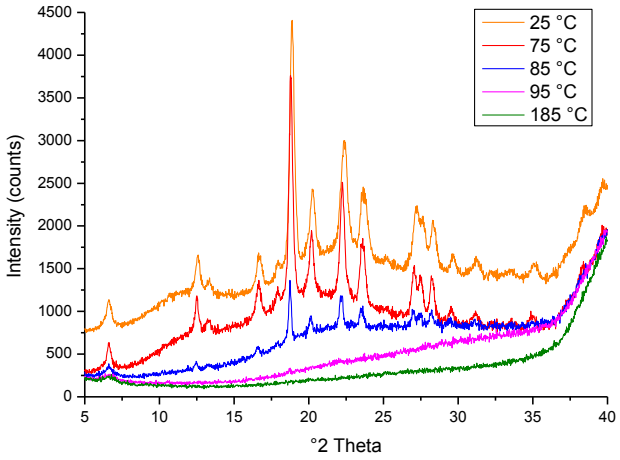


**Fig. 13.** XRPD diffractograms of 35% NAP cryo-milled in combination with PVP. The temperature was increased from 25 °C (orange) to 185 °C (green). Starting from 85 °C (blue) the intensity of the Bragg peaks decreased and from 95 °C (purple), they completely disappeared. The intensities are shown as arbitrary units. (For interpretation of the references to colour in this figure legend, the reader is referred to the web version of this article.)

**Table 3**
Comparison of obtained 'highest drug loadings' based on MDSC or XRPD results in case of cryo-milling.

| Polymer | MDSC | XRPD |
|---|---|---|
| PVP | 50–55% | 15–20% |
| PVP-VA | 30–35% | 10–15% |
| HPMC | < 5% | < 5% |
| HPMC-AS | 10–15% | 5–10% |

On the other hand, these MDSC results show that heat is a very important energy input for these NAP-polymer combinations. Together with the observations form the second heating cycles, where in all cases a single Tg was detected (Figs. 5 and 10), the MDSC experiments were a strong prove that these NAP-polymer combinations do not reach their full potential of miscibility yet. This may be reached by performing a full optimization of the process parameters.

### 3.3.2. *Influence of drug loading on physical structure*

For the NAP-PVP system, the drug loading was increased starting from 35% to 60%. For the other combinations, the drug loading was lowered from 35% to 5%. A full comparison of the highest drug loadings reached per polymer and per manufacturing technique is shown in Table 4.

**Table 4**
Comparison of highest drug loadings of NAP obtained per manufacturing technique and per polymer.

| Technique | Polymer | Drug loading |
|---|---|---|
| Spray drying | PVP | 30–35% |
| | PVP-VA | 40–45% |
| | HPMC | 20–25% |
| | HPMC-AS | 20–25% |
| Hot melt extrusion | PVP | 55–60% |
| | PVP-VA | 45–50% |
| | HPMC | 20–25% |
| | HPMC-AS | 15–20% |
| Cryo-milling | PVP | 15–20% |
| | PVP-VA | 10–15% |
| | HPMC | < 5% |
| | HPMC-AS | 10–15% |

### 3.3.3. *A small scale-up experiment: from 5 mL to 25 mL grinding jar*

All previously described experiments were performed using a small grinding jar of 5 mL. The volume of these stainless steel grinding jars can differ: 5, 10, 25, 35 or 50 mL are possible. When scaling up from a 5 mL to a larger grinding jar volume, the change of dimensions can have an influence on the impact of the beads and thereby the final phase behavior of the ASD. Here, 35% NAP in combination with PVP-VA was cryo-milled in both the 5 mL and the 25 mL for 3 h. The ball to powder ratio was kept constant. At first sight, there is not much difference between the MDSC thermograms of the 5 mL and 25 mL. In both cases, two distinct Tgs indicating amorphous-amorphous phase separation were detected (Fig. 14A). However, the glass transition width was broader when using the 5 mL grinding jar than when using the 25 mL one, indicating that the amorphous phase was more heterogeneous in case of using the 5 mL grinding jar.

Even though the DSC thermograms did not show melting transitions, the diffractogram of the batch prepared with the 5 mL grinding jar showed Bragg peaks characteristic for crystalline NAP (Fig. 14B). As described above, this can be explained by the dissolution of NAP in PVP-VA during the MDSC experiment. Interesting is that the batch prepared with the 25 mL grinding jar was X-ray amorphous (Fig. 14B). This difference was also reflected in the Tg width (Fig. 14A). The fact that there was still some crystalline material present in case of the 5 mL

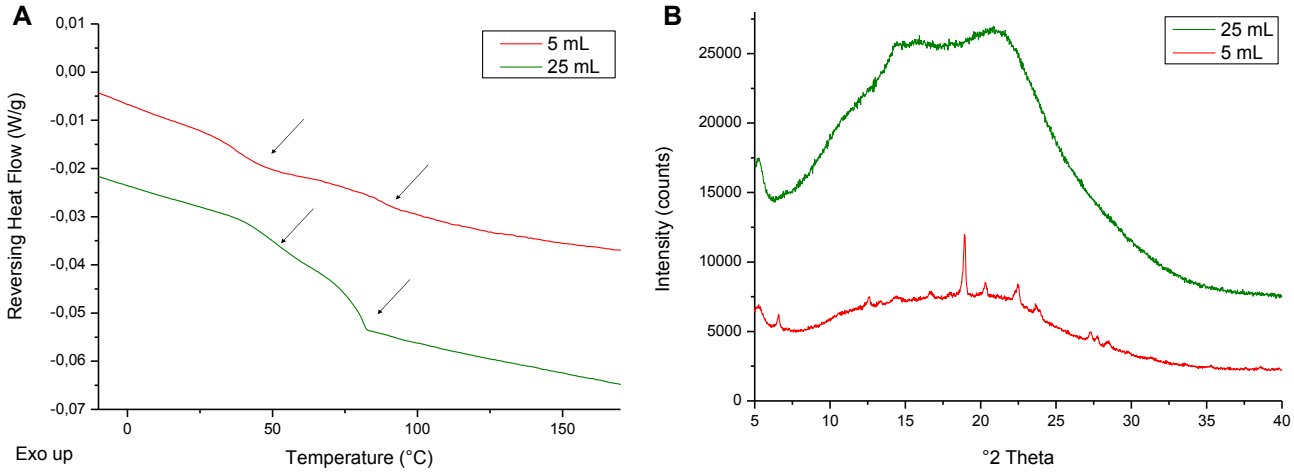


**Fig. 14.** A: MDSC thermograms of 35% NAP cryo-milled in combination with PVP-VA using a 25 mL grinding jar (green) and a 5 mL grinding jar (red). The arrows indicate the position of the Tgs. B: XRPD diffractograms of 35% NAP cryo-milled in combination with PVP-VA using a 25 mL (green) grinding jar and a 5 mL (red) one. The RHF signals (A) and intensities (B) are shown as arbitrary units. (For interpretation of the references to colour in this figure legend, the reader is referred to the web version of this article.)

grinding jar did not prevent dissolving of NAP in PVP-VA, but it resulted in a broader Tg width. In case of the 25 mL grinding jar there was no crystalline material left at the start of the MDSC analysis, resulting in a more homogeneous system compared to the 5 mL one.

This small scale up experiment showed the potential of CM as a manufacturing technique for ASDs. When the larger grinding jar was used, it became possible to prepare systems that were already completely amorphous at RT. Therefore, it can be hypothesized that the optimization of this manufacturing technique could result in higher drug loadings than the ones that were obtained in this study. Next to this, a deeper understanding of the underlying physics of this still non-conventional technique is essential to predict possible changes during scale up.

### 3.4. Comparison

The objective of this study was to prepare the same API-polymer combinations with spray drying, hot melt extrusion and cryo-milling to compare their capability of reaching high drug loadings. The same four NAP-polymer combinations were prepared with all three techniques. For SD and HME, the highest drug loadings were defined as the drug loadings for which a one phase amorphous system was attained, while for CM these were the drug loadings for which an X-ray amorphous ASD was obtained. This distinction was made because of the discrepancy between MDSC and XRPD results for CM, which were not present for SD and HME. Therefore, MDSC can be considered as a reliable technique for the interpretation of the phase behavior in case of SD and HME, but not in case of CM. The drug loadings were determined as described above and reported as a range to consider possible process variation. A full comparison of the highest drug loadings reached per polymer and per manufacturing technique is shown in Table 4.

From these results, it can be stated that HME was the most promising manufacturing technique for obtaining high drug loadings in case of these NAP-polymer combinations. Since HME is a heat based method, this finding is in line with the fact that heat is a very important energy input for these combinations. The correct order of the techniques is as follows: hot melt extrusion > spray drying > cryo-milling. Based on the MDSC results (Table 3), it might have seemed that cryo-milling was as promising as spray drying, but the heat applied during these experiments led to dissolution of NAP in the polymer, leading to the wrong conclusion. Therefore, the reported drug loadings in Table 4 are relatively low drug loadings based on XRPD results. Nevertheless, the scale up from a 5 mL grinding jar to a 25 mL one showed the potential of CM for reaching higher drug loadings than the ones obtained in this study.

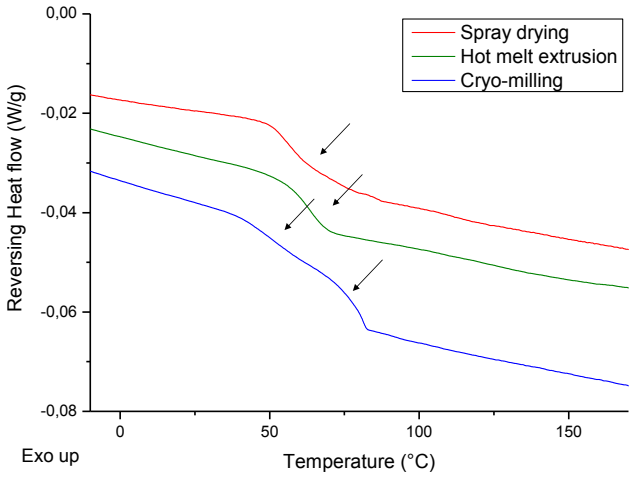


**Fig. 15.** MDSC thermograms of 35% NAP-PVP-VA prepared with all three manufacturing techniques. The arrows indicate the positions of the Tgs. The RHF signals are shown as arbitrary units.

An interesting system to compare the three manufacturing techniques was 35% NAP in combination with PVP-VA. Both in case of HME and SD a single Tg was detected, while in case of CM two Tgs could be distinguished (Fig. 15). The difference between HME and SD exists in the variation of the Tg width. For HME this Tg width was 54.3 °C, while for SD it was 68.1 °C. This shows that the spray dried ASD was more heterogeneous than the extruded one. Although for all techniques 35% NAP in combination with PVP-VA was formulated, clear differences in phase behavior were detected. The most homogeneous system was prepared using HME. This comparison supports the statement that HME is the best manufacturing technique for obtaining high drug loadings in case of these NAP-polymer combinations.

Although there is a clear difference between the NAP-polymer combinations for the drug loadings that could be obtained, there was no ideal polymer for NAP nor per manufacturing technique. Thus, the selection of a polymer depends upon both the API and the technique used. Considering the results in Table 4, the capability to reach high drug loadings is another important characteristic to evaluate when selecting a polymer for the formulation of ASDs.

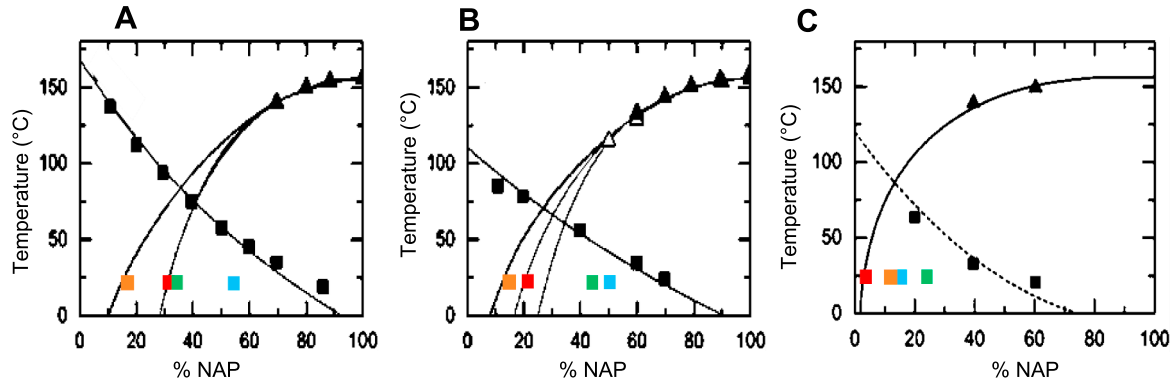


**Fig. 16.** State diagrams of NAP with PVP K25 (A), PVP-VA64 (B) and HPMC-AS (C). The black squares indicate the Tgs and the triangles the solubility of NAP in the polymer. The solubilities were determined experimentally (A, C) or taken from literature (B). Here, the white triangles were derived from Kyerematenget al. [29] and the black ones from Prudic et al. [30]. For PVP and PVP-VA, Flory-Huggings and an empirical model were applied as well. The solubilities calculated with PC-SAFT are indicated with red squares, showing the solubility of NAP in the polymer at RT. The highest drug loadings reached with spray drying (green), hot melt extrusion (blue) and cryo-milling (orange) are indicated. Reprinted (adapted) with permission from Lehmkemper et al. [11] *'Impact of Polymer Type and Relative Humidity on the Long-Term Physical Stability of Amorphous Solid Dispersions', Molecular Pharmaceutics, 14(12), pp. 4374–4386.* Lehmkemper et al. [12] *'Long-Term Physical Stability of PVP- and PVPVA-Amorphous Solid Dispersions', Molecular Pharmaceutics, 14(1), pp. 157–171).* Copyright 2017 American Chemical Society. (For interpretation of the references to colour in this figure legend, the reader is referred to the web version of this article.)

The distinction between thermodynamic stabilization and kinetic stabilization becomes clear when comparing these drug loadings with the ones calculated with PC-SAFT. As described earlier, the solubility of the API in the polymer can be calculated using PC-SAFT. Lehmkemper et al. [11,12] determined the thermodynamic solubility of NAP in PVP-VA, PVP and HPMC-AS. This resulted in the following maximum drug loadings at room temperature: 20.7% for PVP-VA, 31.4% for PVP and 3% for HPMC-AS (Figs. 2 and 16). Here, higher drug loadings were reached with PVP-VA and HPMC-AS for both HME and spray drying, because of kinetic trapping (Fig. 16). In a SD process, the feed solution is atomized in droplets, followed by mixing of the droplets with the drying gas. The drying rate can be a critical factor for amorphization. The solvent evaporation should be rapid enough to kinetically trap the API in the polymer matrix. Thereby the API does not have the time to crystallize during processing. Thus, the drying kinetics should be controlled to make preparation of completely amorphous ASDs feasible [13]. In a HME process, both the installed barrel temperature and applied shear forces heat the sample. When exiting the die, the mixture is rapidly cooled, which should be fast enough to kinetically trap the API in the polymer matrix. These are two different mechanisms that both result in kinetic trapping of the API in the polymer matrix. As becomes clear from the results in Table 4, these mechanisms make it possible to reach higher drug loadings than thermodynamically predicted. In case of PVP, higher drug loadings could be reached using HME, but in case of SD the calculated drug loading of 31.4% was in between the experimentally determined range of 30–35% (Fig. 16A). Here, it was not possible to reach higher drug loadings, but at least the calculated drug loading was reached. This shows that the thermodynamic solubility can be considered as the minimum drug loading that should be achieved at a certain temperature. Since this minimum drug loading was not yet reached for the NAP-PVP and PVP-VA combinations using cryo-milling, an optimization of the process is required.

This study showed clear differences between spray drying, hot melt extrusion and cryo-milling for their capability to reach high drug loadings. In all cases, the conventional process parameters were used. Except for the alterations of the barrel temperature in case of HME, no optimization was performed. This implies that the drug loadings reported here may be increased when a full optimization of the process parameters is carried out. For SD, the drying air temperature, drying air flow rate, feed solution flow rate and atomization air flow rate should be optimized. For HME the important process parameters are the screw speed, screw configuration, barrel temperature and the feed rate. In case of CM, the filling level in the milling chamber, the milling frequency, the milling time and the beads combination should be optimized. Even though a full optimization may show even more potential for reaching higher drug loadings for all manufacturing techniques, this study defined the potential differences between the techniques. It can be stated that although the starting material is chemically identical, the final products will be physically different when applying a technology from a different category of manufacturing techniques.

## 4. Conclusion

In this study, four NAP-polymer combinations were prepared using spray drying, hot melt extrusion and cryo-milling. By comparing these three technologies, all three categories of manufacturing techniques were covered. The same drug loading of 35% was pursued for all NAP-polymer combinations and every technique. Where PVP-VA was the best polymer for SD, PVP and PVP-VA were both promising for HME and PVP showed the best results in case of CM. This showed that there is no ideal NAP-polymer combination that could be applied for every manufacturing technique. The selection of carrier should be made per API and per technique. More importantly, the highest drug loadings feasible for all combinations were established per technique. Therefrom, it can be concluded that HME was the best manufacturing technique for reaching high drug loadings in case of these NAP-polymer combinations. This is in agreement with the importance of heat as an energy input for these systems. By full optimization of the process parameters even higher drug loadings might be obtained than described here in the article, yet robustness will need to be proven as the manufacturing process is scaled and undergoes the full manufacturing variation. Next to this, it was shown that higher drug loadings could be reached by kinetically trapping NAP in the polymer matrix than was predicted based on thermodynamics. Since this kinetic stabilization can minimize the molecular mobility to an acceptable low level, it is also essential for obtaining an appropriate shelf life. In addition, the biopharmaceutical performance, manufacturability and chemical stability should be considered.

## Acknowledgements

Laboratoires SMB and Het Fonds voor Wetenschappelijk Onderzoek-Vlaanderen (FWO) are acknowledged for support. The authors would like to thank Prof. Bart Goderis (Polymer Chemistry and Materials, KU Leuven) and Prof. Peter Van Puyvelde (Chemical Engineering, KU Leuven) for technical assistance.

## References


[1] C.A. Lipinski, F. Lombardo, B.W. Dominy, P.J. Feeney, Experimental and computational approaches to estimate solubility and permeability in drug discovery and development settings, Adv. Drug Deliv. Rev. 23 (1997) 3–25, https://doi.org/10.1016/S0169-409X(00)00129-0.

[2] H.D. Williams, N.L. Trevaskis, S.A. Charman, R.M. Shanker, W.N. Charman, C.W. Pouton, C.J.H. Porter, Strategies to address low drug solubility in discovery and development, Pharmacol. Rev. 65 (2013) 315–499, https://doi.org/10.1124/pr.112.005660.

[3] R.O. Williams, A.B. Watts, D.A. Miller, Formulating Poorly Water Soluble Drugs, Springer, 2012.

[4] G. Van Den Mooter, The use of amorphous solid dispersions: a formulation strategy to overcome poor solubility and dissolution rate, Drug Discov. Today Technol. 9 (2012) e79–e85, https://doi.org/10.1016/j.ddtec.2011.10.002.

[5] S. Janssens, G. Van den Mooter, Review: physical chemistry of solid dispersions, J. Pharm. Pharmacol. 61 (2009) 1571–1586, https://doi.org/10.1211/jpp/61.12.0001.

[6] K. Edueng, D. Mahlin, C.A.S. Bergström, The need for restructuring the disordered science of amorphous drug formulations, Pharm. Res. 34 (2017) 1754–1772, https://doi.org/10.1007/s11095-017-2174-7.

[7] S. Navnit, S. Harpreet, C. Duk Soon, C. Hitesh, A.M. Waseem, Amorphous Solid Dispersions, Springer, New Jersey, 2014.

[8] N. Kang, J. Lee, J.N. Choi, C. Mao, E.H. Lee, Cryomilling-induced solid dispersion of poor glass forming/poorly water-soluble mefenamic acid with polyvinylpyrrolidone K12, Drug Dev. Ind. Pharm. 41 (2015) 978–988, https://doi.org/10.3109/03639045.2014.920024.

[9] T. Vasconcelos, S. Marques, J. das Neves, B. Sarmento, Amorphous solid dispersions: rational selection of a manufacturing process, Adv. Drug Deliv. Rev. 100 (2016) 85–101, https://doi.org/10.1016/j.addr.2016.01.012.

[10] S. Bangalore, G. Kamalakkannan, S. Parkar, F.H. Messerli, Fixed-dose combinations improve medication compliance: a meta-analysis, Am. J. Med. 120 (2007) 713–719, https://doi.org/10.1016/j.amjmed.2006.08.033.

[11] K. Lehmkemper, S.O. Kyerematen, O. Heinzerling, M. Degenhardt, G. Sadowski, Impact of polymer type and relative humidity on the long-term physical stability of amorphous solid dispersions, Mol. Pharm. 14 (2017) 4374–4386, https://doi.org/10.1021/acs.molpharmaceut.7b00492.

[12] K. Lehmkemper, S.O. Kyerematen, O. Heinzerling, M. Degenhardt, G. Sadowski, Long-term physical stability of PVP- and PVPVA-amorphous solid dispersions, Mol. Pharm. 14 (2017) 157–171, https://doi.org/10.1021/acs.molpharmaceut.6b00763.

[13] A. Singh, G. Van den Mooter, Spray drying formulation of amorphous solid dispersions, Adv. Drug Deliv. Rev. 100 (2016) 27–50, https://doi.org/10.1016/j.addr.2015.12.010.

[14] K. Sekiguchi, N. Obi, Y. Ueda, Studies on absorption of eutectic mixture. II. Absorption of fused conglomerates of chloramphenicol and urea in rabbits, Chem. Pharm. Bull. (Tokyo) 12 (1964) 134–144, https://doi.org/10.1248/cpb.12.134.

[15] B. Van Eerdenbrugh, S. Raina, Y.-L. Hsieh, P. Augustijns, L.S. Taylor, Classification of the crystallization behavior of amorphous active pharmaceutical ingredients in aqueous environments, Pharm. Res. 31 (2014) 969–982, https://doi.org/10.1007/s11095-013-1216-z.

[16] A. Jubert, M.L. Legarto, N.E. Massa, L.L. Tévez, N.B. Okulik, Vibrational and theoretical studies of non-steroidal anti-inflammatory drugs Ibuprofen [2-(4-isobutylphenyl)propionic acid]; Naproxen [6-methoxy-α-methyl-2-naphthalene acetic acid] and Tolmetin acids [1-methyl-5-(4-methylbenzoyl)-1H-pyrrole-2-acetic acid], J. Mol. Struct. 783 (2006) 34–51, https://doi.org/10.1016/j.molstruc.2005.08.018.

[17] M.M. Velazquez, M. Valero, L.J. Rodríguez, S.M.B. Costa, M.A. Santos, Hydrogen bonding in a non-steroidal anti-inflammatory drug-Naproxen, J. Photochem. Photobiol. B Biol. 29 (1995) 23–31, https://doi.org/10.1016/1011-1344(95)90245-7.

[18] A. Paudel, J. Van Humbeeck, G. Van Den Mooter, Theoretical and experimental investigation on the solid solubility and miscibility of naproxen in poly (vinylpyrrolidone), Mol. Pharm. 7 (2010) 1133–1148, https://doi.org/10.1021/mp100013p.

[19] B. Van Eerdenbrugh, L.S. Taylor, An ab initio polymer selection methodology to prevent crystallization in amorphous solid dispersions by application of crystal engineering principles, CrystEngComm 13 (2011) 6171–6178, https://doi.org/10.1039/c1ce05183k.

[20] D.T. Friesen, R. Shanker, M. Crew, D.T. Smithey, W.J. Curatolo, J.A.S. Nightingale, Hydroxypropyl methylcellulose acetate succinate-based spray spray-dried dispersions: an overview 5 (2008) 1003–1019.

[21] M.A. Repka, S. Bandari, V.R. Kallakunta, A.Q. Vo, H. McFall, M.B. Pimparade, A.M. Bhagurkar, Melt extrusion with poorly soluble drugs – an integrated review, Int. J. Pharm. 535 (2018) 68–85, https://doi.org/10.1016/j.ijpharm.2017.10.056.

[22] J. Thiry, F. Krier, B. Evrard, A review of pharmaceutical extrusion: critical process parameters and scaling-up, Int. J. Pharm. 479 (2015) 227–240, https://doi.org/10.1016/j.ijpharm.2014.12.036.

[23] Y. Shibata, M. Fujii, Y. Sugamura, R. Yoshikawa, S. Fujimoto, S. Nakanishi, Y. Motosugi, N. Koizumi, M. Yamada, K. Ouchi, Y. Watanabe, The preparation of a solid dispersion powder of indomethacin with crospovidone using a twin-screw extruder or kneader, Int. J. Pharm. 365 (2009) 53–60, https://doi.org/10.1016/j.ijpharm.2008.08.023.

[24] R.C. Rowe, P.J. Sheskey, M.E. Quinn, Handbook of Pharmaceutical Excipients, Pharmaceutical Press, 2009.

[25] K. Nakamichi, T. Nakano, H. Yasuura, S. Izumi, Y. Kawashima, The role of the kneading paddle and the effects of screw revolution speed and water content on the preparation of solid dispersions using a twin-screw extruder, Int. J. Pharm. 241 (2002) 203–211, https://doi.org/10.1016/S0378-5173(02)00134-5.

[26] L. Saerens, L. Dierickx, T. Quinten, P. Adriaensens, R. Carleer, C. Vervaet, J.P. Remon, T. De Beer, In-line NIR spectroscopy for the understanding of polymer-drug interaction during pharmaceutical hot-melt extrusion, Eur. J. Pharm. Biopharm. 81 (2012) 230–237, https://doi.org/10.1016/j.ejpb.2012.01.001.

[27] B. Lang, J.W. McGinity, R.O. Williams, Dissolution enhancement of itraconazole by hot-melt extrusion alone and the combination of hot-melt extrusion and rapid freezing-effect of formulation and processing variables, Mol. Pharm. 11 (2014) 186–196, https://doi.org/10.1021/mp4003706.

[28] D. Bikiaris, G.Z. Papageorgiou, A. Stergiou, E. Pavlidou, E. Karavas, F. Kanaze, M. Georgarakis, Physicochemical studies on solid dispersions of poorly water-soluble drugs: evaluation of capabilities and limitations of thermal analysis techniques, Thermochim. Acta 439 (2005) 58–67, https://doi.org/10.1016/j.tca.2005.09.011.

[29] S.O. Kyerematen, M. Pudlas, G.H. Woehrle, A fast and reliable empirical approach for estimating solubility of crystalline drugs in polymers for hot melt extrusion formulations, J. Pharm. Sci. 103 (2014) 2847–2858, https://doi.org/10.1002/jps.23941.

[30] A. Prudic, T. Kleetz, M. Korf, Y. Ji, G. Sadowski, Influence of copolymer composition on the phase behavior of solid dispersions, Mol. Pharm. 11 (2014) 4189–4198, https://doi.org/10.1021/mp500412d.